韓國海洋工學會誌 第11卷 第1號, pp.65~73, 1997. 2

◉ 論 文

Wave Control Function and Friction Damping of a Pile-Supported Floating Body

Heon-Tae Kim*

(97년 1월 7일 접수)

말뚝계류식 부유체의 파랑제어 기능과 마찰감쇠에 관한 연구

김 헌 태*

Key Words : Pile-Supported Floating Body(말뚝계류식 부유체), Floating Structure(부유식 구조물), Offshore Structure (해양구조물), Friction Damping(마찰감쇠), Coulomb Friction(쿨롬마찰), Equivalent Damping Coefficient(등가감쇠계수)

초 록

본 연구는 부유식 파랑제어구조물의 계류방식을 말뚝계류식으로 하여 종래의 부유식 파랑제어구조물의 파랑제어기능을 보완하고, 친수성 구조물로 이용할 수 있는 다용도 구조물의 개발을 목표로 하고 있다. 본 연구에서는 부유체의 계류장치에 초기반력을 작용시킴으로써 발생하는 파랑제어 효과의 개선과 부유체의 동요제어 효과를 수치계산법을 통하여 논의하였다. 이때 계류부에서 발생하는 비선형 마찰력을 운동방정식에 고려하여 전개하는 한편, 계산의 효율화를 위하여 비선형 마찰력을 선형모델화하는 이론을 전개한 다음 수치계산 및 실험값을 통하여 본 수치모델의 적용성에 관하여 논의한 결과 양호한 일치성을 보였다. 또한, 파랑제어 효과 및 부유체의 동요저감 효과를 동시에 만족할 수 있는 초기반력에 관하여 논의하였다.

1. INTRODUCTION

The floating body discussed in this study is a 2-D rectangular floating unit supported by four vertical piles at its corners. Structures of this type are frequently seen as floating piers for the crafts in a small harbour. The movement in some modes of motion of such a floating body is fully or partially restricted by the piles. The authors (Kim et al. 1994) carried out a series of model tests on its wave control function, its motions and the loads on piles. The experimental results showed that a certain degree of initial constriction force which clamps the floating unit in the horizontal direction can effectively reduce the body motions and wave energy without increasing mooring forces. This may be due to the friction forces occurring

* School of Ocean Eng., Pukyong National Univ.

between the piles and the rollers installed in the mooring equipments on the floating unit.

In this paper, we develop a numerical model for the prediction of wave transformation and floating body motions, where the friction force is idealized as the Coulomb friction and linearized into a damping force using the equivalent damping coefficient. This linearization is verified by comparing the results of motions between the linear and nonlinear analysis of the equations of motion. We further compare the calculation results by the linear model with the experimental results and discuss the effect of the friction force or the constriction force on body motions and wave energy dissipation.

2. THEORETICAL FORMULATION

2.1 Equations of Motion

Fig. 1 shows a schematic diagram of a floating body moored to the piles with linear springs and rollers. The friction between the rollers and the piles is assumed to be the Coulomb friction that gives constant friction force proportional to the restoring force of the spring in the opposite direction to the moving direction of the rollers.

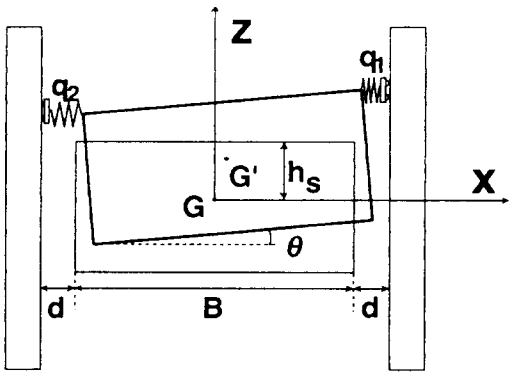

Fig. 1 Schematic diagram of a floating body supported by piles

Let three modes of motion in two dimensions with respect to the centre of gravity G be sway, heave and roll and express the displacements by x, z and θ, respectively.

The equations of motion are obtained as follows assuming the small amplitude motion under the excitation of sinusoidal waves:

$$\text{sway: } (m+M_{11})\ddot{x}+M_{13}\ddot{\theta}+N_{11}\dot{x}+N_{13}\dot{\theta} = aF_1^*\cos(\omega t+\varepsilon_1)-2k(x-h_s\theta) \quad (1)$$

$$\text{heave: } (m+M_{22})\ddot{z}+N_{22}\dot{z}+C_{22}z = aF_2^*\cos(\omega t+\varepsilon_2)-fk\{V_1(s-h_s\theta+x)+V_2(s+h_s\theta-x)\} \quad (2)$$

$$\text{roll: } (I+M_{33})\ddot{\theta}+M_{31}\ddot{x}+N_{33}\dot{\theta}+N_{31}\dot{x}+C_{33}\theta = aF_3^*\cos(\omega t+\varepsilon_3)+k(-2h_s^2\theta+2h_sx) -0.5fkB'\{V_1(s-h_s\theta+x)-V_2(s+h_s\theta-x)\} \quad (3)$$

where m and I are the mass and the inertia moment of the floating body, and M and N are the added mass and the damping coefficient, respectively. C is the hydrostatic restoring force coefficient, a is the wave amplitude, f is the friction coefficient, ε is the phase lag, and $B'=B+2d$. The numerals in the subscripts 1, 2 and 3 indicate the corresponding modes of motion, sway, heave and roll, respectively. F^* is the transfer function of wave force that is a function of wave frequency like the added mass and the damping coefficients. k is the spring constant and s is the initial displacement of the spring defined as $F_o=ks$ where F_o is the initial constriction force. There is an important assumption here that the initial constriction must be large enough not to detach the rollers from the piles. This assumption is not always fulfilled

in the experiments especially for the cases of small constriction forces. The coefficients V_1 and V_2 in Eqs. (2) and (3) take the value of 1 or -1 according to the moving direction of the rollers. Thus these are given as

$$V_1 = (\dot{z} + \dot{\theta}B'/2)/|\dot{z} + \dot{\theta}B'/2|\ ,$$
$$V_2 = (\dot{z} - \dot{\theta}B'/2)/|\dot{z} - \dot{\theta}B'/2| \qquad (4)$$

2.2 Nonlinear Analysis

We introduce the following dimensionless variables to treat the equations of motion in dimensionless form:

$$X = x/a\ ,\ Z = z/a\ ,\ \Theta = \theta B/a\ ,\ \tau = \omega t$$
$$\mu_{13} = M_{13}/(m+M_{11})B,\quad \mu_{31} = M_{31}B/(I+M_{33})$$
$$\lambda_{11} = N_{11}/(m+M_{11})\omega,\quad \lambda_{13} = N_{13}/(m+M_{11})B\omega,$$
$$\lambda_{22} = N_{22}/(m+M_{22})\omega,\quad \lambda_{31} = N_{31}B/(I+M_{33})\omega,$$
$$\lambda_{33} = N_{33}/(I+M_{33})\omega,\quad \zeta_{11} = 2k/(m+M_{11})\omega^2,$$
$$\zeta_{13} = -2kh_s/(m+M_{11})B\omega^2,\ \zeta_{22} = C_{22}/(m+M_{22})\omega^2$$
$$\alpha_1 = F_1^*/(m+M_{11})\omega^2,\ \alpha_2 = F_2^*/(m+M_{22})\omega^2,$$
$$\alpha_3 = F_3^*B/(I+M_{33})\omega^2$$

Furthermore, we divide the velocity phase plane $Z-\Theta$ into the following four regions within which the signs of V_1 and V_2 are constant:

region 1: $\dot{Z} \geq |\dot{\Theta}|B'/2B \quad (V_1 = V_2 = 1)$

region 2: $\dot{\Theta}B'/B \geq 2|\dot{Z}| \quad (V_1 = 1,\ V_2 = -1)$

region 3: $\dot{Z} \leq -|\dot{\Theta}|B'/2B \quad (V_1 = V_2 = -1)$

region 4: $\dot{\Theta}B'/B \leq -2|\dot{Z}| \quad (V_1 = -1,\ V_2 = 1)$

where the dots indicate the differentiation with respect to time. In addition to the parameters shown above, the following dimensionless parameters that take different expressions in each region are defined where the numerals in the superscript denote the region number:

$$\zeta_{21}^{(1)} = \zeta_{21}^{(3)} = 0,\ \zeta_{21}^{(2)} = 2fk/(m+M_{22})\omega^2,\ \zeta_{21}^{(4)} = -\zeta_{21}^{(2)}$$
$$\zeta_{23}^{(1)} = \zeta_{23}^{(3)} = 0,\quad \zeta_{23}^{(2)} = -2fkh_s/(m+M_{22})B\omega^2,$$
$$\zeta_{23}^{(4)} = -\zeta_{23}^{(2)}$$
$$\zeta_{31}^{(1)} = -(2kh_sB - fkBB')/(I+M_{33})\omega^2\ ,$$
$$\zeta_{31}^{(2)} = -2k_sB'/(I+M_{33})\omega^2$$
$$\zeta_{31}^{(3)} = -(2kh_sB + fkBB')/(I+M_{33})\omega^2\ ,$$
$$\zeta_{31}^{(4)} = \zeta_{31}^{(2)}$$
$$\zeta_{33}^{(1)} = (C_{33} + 2kh_s^2 - fkh_sB')/(I+M_{33})\omega^2\ ,$$
$$\zeta_{33}^{(2)} = (C_{33} + 2kh_s^2)/(I+M_{33})\omega^2$$
$$\zeta_{33}^{(3)} = (C_{33} + 2kh_s^2 + fkh_sB')/(I+M_{33})\omega^2\ ,$$
$$\zeta_{33}^{(4)} = \zeta_{33}^{(2)}$$
$$\gamma_2^{(1)} = -2fF_0/(m+M_{22})a\omega^2\ ,\quad \gamma_2^{(2)} = \gamma_2^{(4)} = 0\ ,$$
$$\gamma_2^{(3)} = -\gamma_2^{(1)}$$
$$\gamma_3^{(1)} = \gamma_3^{(3)} = 0\ ,\quad \gamma_3^{(2)} = -fF_0BB'/(m+M_{33})a\omega^2\ ,$$
$$\gamma_3^{(4)} = -\gamma_3^{(2)}$$

Using these parameters we obtain the dimensionless equation of motions in matrix form, where n takes 1 to 4:

$$\begin{pmatrix} 1 & 0 & \mu_{13} \\ 0 & 1 & 0 \\ \mu_{31} & 0 & 1 \end{pmatrix} \begin{pmatrix} \ddot{X} \\ \ddot{Z} \\ \ddot{\Theta} \end{pmatrix} + \begin{pmatrix} \lambda_{11} & 0 & \lambda_{13} \\ 0 & \lambda_{22} & 0 \\ \lambda_{31} & 0 & \lambda_{33} \end{pmatrix} \begin{pmatrix} \dot{X} \\ \dot{Z} \\ \dot{\Theta} \end{pmatrix}$$
$$+ \begin{pmatrix} \zeta_{11} & 0 & \zeta_{13} \\ \zeta_{21}^{(n)} & \zeta_{22} & \zeta_{23}^{(n)} \\ \zeta_{31}^{(n)} & 0 & \zeta_{33}^{(n)} \end{pmatrix} \begin{pmatrix} X \\ Z \\ \Theta \end{pmatrix} = \begin{pmatrix} a_1\cos(\tau+\varepsilon_1) \\ a_2\cos(\tau+\varepsilon_2) \\ a_3\cos(\tau+\varepsilon_3) \end{pmatrix} + \begin{pmatrix} 0 \\ \gamma_2^{(n)} \\ \gamma_3^{(n)} \end{pmatrix} \qquad (5)$$

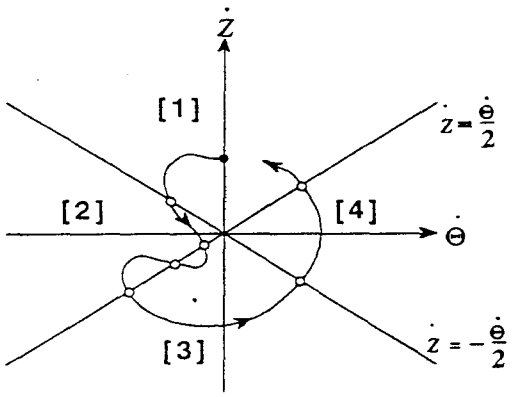

Fig. 2 Divided regions and boundaries for the nonlinear calculation

Since the equations of motion are linear differential equations within each region, we can obtain the analytical solution in each region by specifying the initial displacements and velocities in the three modes of motion. Thus as shown in Fig. 2 we proceed with the calculation starting from any point on the velocity phase plane $Z-\Theta$. The subsequent motions are calculated at successive time steps from the corresponding analytical solutions up to the instant at which the locus reaches the boundary of the region. The analytical solutions for the subsequent region is then used, with the unknown coefficients determined from the values of displacements and velocities at the cross-over. This procedure is extended over the required duration. All the calculation performed in this study take the initial conditions as $(Z,\Theta)=(0,0)$ and $(Z,\Theta)=(0,0.1)$ in the region 1 although different initial conditions could give different solutions due to the nonlinearity. The Laplace transformation is used to get analytical solutions by the help of Mathematica. Fig. 3 shows an example of the locus, which shows higher harmonic components due to the friction effect.

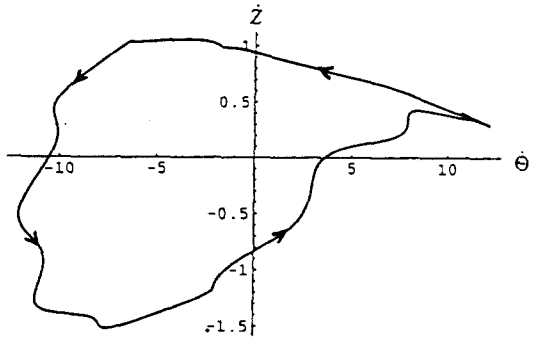

Fig. 3 Locus on velocity phase plane

In this nonlinear analysis, the wave exciting force, the added mass and the damping coefficients must be calculated beforehand by using the linear potential theory. The nonlinear analysis is thus unable to predict the wave field directly. Furthermore, the conversion characteristics at the cross-over point become sometimes worse as the initial constriction or the friction factor become large. We therefore use the nonlinear analysis for only verifying the validity of the linearized theory referred to in the next section.

2.3 Linearization of Nonlinear Friction Force using Equivalent Damping Coefficient

The Coulomb friction force is described as a step function of velocity as shown in Fig. 4 (a). We here linearize this nonlinear function as a straight line shown in Fig. 4 (b), where we replace the friction force with the linear damping force due to a dash-pot. To determine the slope of the line or the damping coefficient, we equate the total dissipating energy during one wave period due to the friction force with that due to the damping force.

The total dissipating energy E_f due to the friction force F_f during one wave period T is calculated as

$$E_f = \int_0^T F_f v dt = 4\int_0^{\pi/2} \frac{F_0 v_0}{\omega} \cos\theta d\theta = \frac{4F_0 v_0}{\omega} \tag{6}$$

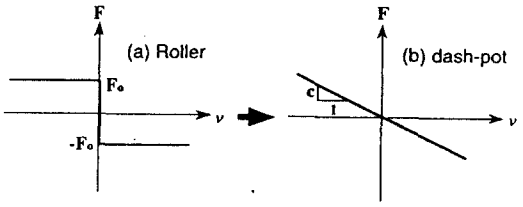

Fig. 4 Coulomb friction (a) and its linearization (b)

On the other hand, the total dissipating energy E_d due to the damping force F_d is

$$E_d = \int_0^T F_d v dt = \int_0^{2\pi} \frac{c v_0^2}{\omega} \cos^2\theta d\theta = \frac{c v_0^2 \pi}{\omega} \tag{7}$$

To equate E_f with E_d, we obtain the equivalent damping coefficient c as

$$c = 4F_0 / v_0 \pi \tag{8}$$

We here notice that the equivalent damping coefficient c is determined by the magnitude of the friction force F_0 and the velocity amplitude of the rollers v_0. However, the velocity of the rollers is in turn a function of the damping coefficient. Thus in the calculation we first assume a damping coefficient and calculate the first approximate value of v_0 and then modify the damping coefficient by using Eq. (8). This procedure is iterated until the steady-state value of c is obtained.

Considering the present situation shown in Fig. 7, however, there are two rollers on both sides of the floating body. We thus determine the equivalent damping coefficients simultaneously on both sides. Let the equivalent damping coefficients be c_1 and c_2 on the left and right hand sides, respectively. The friction terms on the right hand sides in Eqs. (2) and (3) can be written as

$$-fk\{V_1(s-h_s\theta+x)+V_2(s+h_s\theta-x)\} = -c_1(\dot{z}+\dot{\theta}B'/2)-c_2(\dot{z}-\dot{\theta}B'/2) \tag{9}$$

$$-fkB'\{V_1(s-h_s\theta+x)-V_2(s+h_s\theta-x)\}/2 = -c_1B'(\dot{z}+\dot{\theta}B'/2)/2-c_2(\dot{z}-\dot{\theta}B'/2)/2 \tag{10}$$

If we here let $b_{22}=c_1+c_2$, $b_{23}=b_{32}=B'(c_1-c_2)/2$, $b_{23}=B'^2(c_1+c_2)/4$, Eqs. (2) and (3) yield the following differential equations:

$$(m+M_{22})\ddot{z}+(N_{22}+b_{22})\dot{z}+b_{23}\dot{\theta}+C_{22}z = aF_2^*\cos(\omega t+\varepsilon_2) \tag{11}$$

$$(I+M_{33})\ddot{\theta}+M_{31}\ddot{x}+(N_{33}+b_{33})\dot{\theta}+N_{31}\dot{x}+b_{32}\dot{z}+C_{33}\theta = aF_3^*\cos(\omega t+\varepsilon_3)+k(-2h_s^2\theta+2h_s x) \tag{12}$$

2.4 Numerical Procedure

The linear equations of motion, Eqs. (1), (11), and (12), can be used as the dynamic boundary conditions when solving the boundary-value problem of the wave field. Figure 11 shows a schematic diagram of a vertical section of the floating body used in the experiments. The numerical method used in the calculation is one of the eigenfunction expansion methods proposed by Yoshida et al. (1990). We first divide the water region of interest into five sub-regions as shown in Fig. 5 and then apply the continuity conditions of pressure and velocity on the vertical boundaries between the regions. Solving the equations of motions and the continuity conditions simultaneously, we finally obtain the

amplitudes of motions and the values of unknown coefficients of the velocity potential in each region. As mentioned above, however, the coefficients b_{22}, b_{23}, b_{32} and b_{33} that represent the equivalent damping are also unknown. We first let all these coefficients be zero as first approximations and solve the equations and get the second approximations through Eq. (8). Steady-state solutions can be obtained in several times of such iterations.

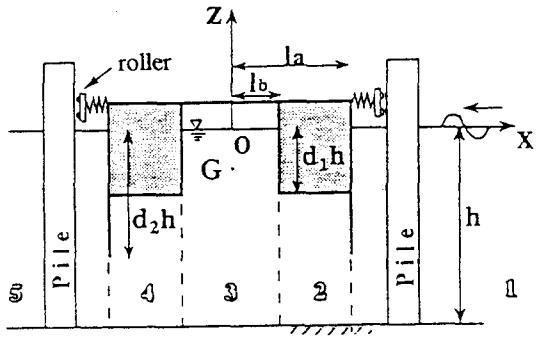

Fig. 5 Subdivision of the fluid region

3. RESULTS

3.1 Comparison between Linear and Nonlinear Analysis

Fig. 6 shows the response of roll amplitudes as a function of wave period T, where the width and the draft of the rectangular floating body are 0.35m and 0.1m, respectively, and the water depth h=0.5m, k=10kgf/cm, f=0.2 and F_o=0.5kgf. The results from the linear model with and without damping are compared to those from the nonlinear model. The linear model considering the equivalent damping show good agreement with the nonlinear model. We also notice the significant effect of the friction damping at the resonant period of the roll motion.

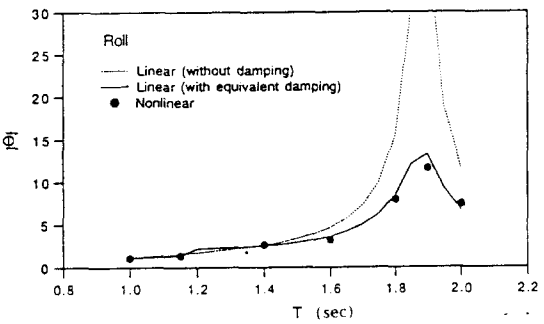

Fig. 6 Comparison of roll amplitudes between linear and nonlinear analysis

3.2 Effects of Friction Damping on Wave Energy Dissipation and Motions

Fig. 7 to Fig. 9 show the comparisons between the calculations and the experiments in terms of the transmission coefficient K_t, the heave and roll amplitudes $|Z|$ and $|\Theta|$, respectively, where the initial constriction force R_X is 3.5kgf, i.e. the initial deflection of the leaf spring s is 0.123cm. We determined the value of the friction coefficient f as 0.2 that corresponds to the maximum static resistance of the roller against its rolling. From these figures, the calculated results show some distinct peaks in the response curves, whereas the experimental results show gradual variation over the tested range of B/L, where L is the wave length. The discrepancy between them is therefore significant around the B/L at which the calculated response curves show the peaks. This may be partly because the friction force between the rollers and the piles is not so simple as it can be idealized as the Coulomb friction and partly because the assumptions used in the model such as small amplitude motion and no detachment of the rollers from the piles may collapse around the frequency showing the peaks.

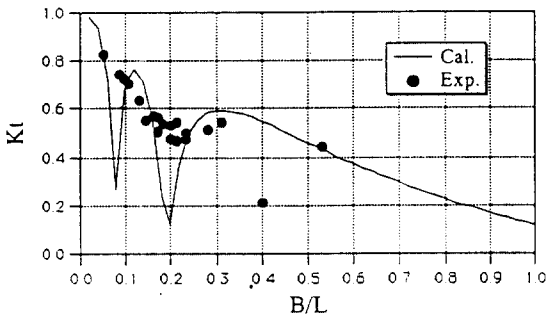

Fig. 7 Transmission coefficient

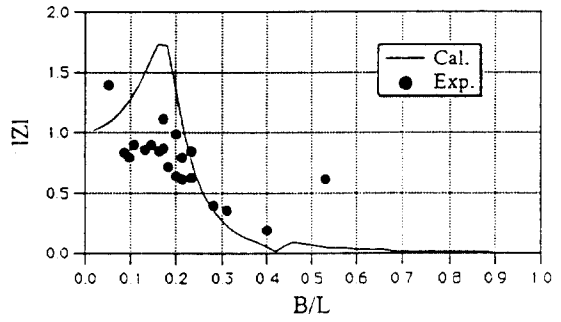

Fig. 8 Heave amplitude

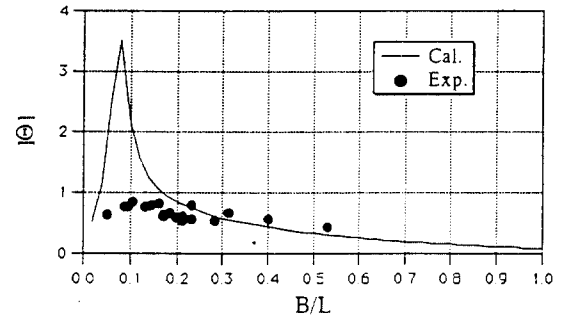

Fig. 9 Roll amplitude

Fig. 10 shows the energy dissipation rate E_L defined as $E_L = 1 - K_t^2 - K_r^2$ where K_t and K_r are the transmission and reflection coefficients, respectively. Experimental results show large energy dissipation around B/L=0.2 for the cases of smaller initial deflections of leaf springs, s=0.123 and s=0.211cm, which respectively correspond to the initial constriction forces R_N = 3.5 and 6.0kgf. On the other hand, the calculations show completely opposite results; the largest initial constriction, s=0.518cm, gives the greatest energy dissipation although the variation characteristics of the response curves are similar to those of the experiments.

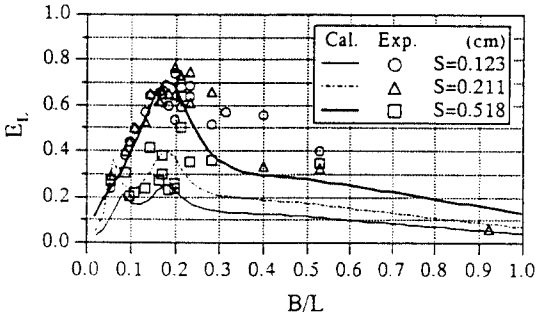

Fig. 10 Energy dissipation rate for three different initial constriction forces

Fig. 11 shows the dependencies of K_t, K_r and E_L on the initial deflection of the spring s or the initial constriction force. In this figure, the experimental results are plotted for the cases B/L=0.14 and 0.16, compared with the results calculated for B/L=0.15. As have seen in Fig. 10, the energy dissipation rate in the experiments decreases with s increasing, whereas the calculated results increase as s increases. It is seen that this opposite tendency corresponds to the variation of the reflection coefficient. In Fig. 12, the amplitudes of heave and sway motions are plotted as functions of s, which shows similar tendency but significant discrepancy between the experiments and the calculations. Fig. 13 and Fig. 14 are the similar figures to Figs. 11 and 12, respectively, except that the calculations are carried out using larger friction coefficient f=0.5. The response curves in Fig. 13 are significantly different from those in Fig. 11. The calculation results show that the optimum constriction force

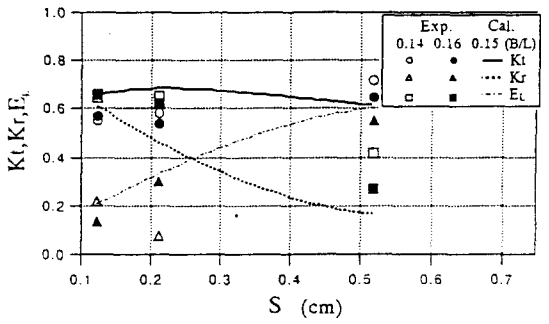

Fig. 11 Transmission coefficient Kt, reflection coefficient Kr and energy dissipation rate E_L as functions of initial deflection of spring s (f=0.2)

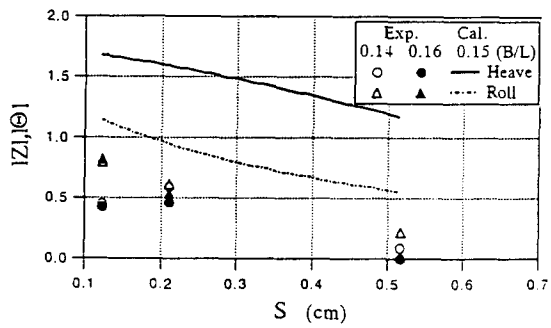

Fig. 12 Heave and roll amplitudes as functions of initial deflection of spring s (f=0.2)

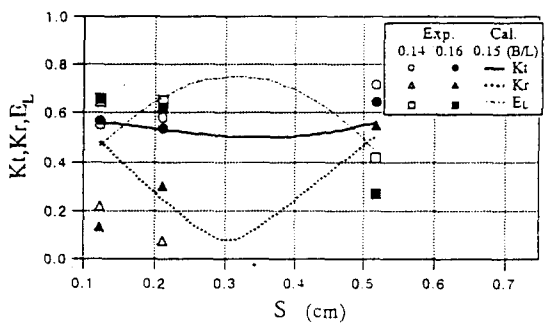

Fig. 13 Transmission coefficient Kt, reflection coefficient Kr and energy dissipation rate E_L as functions of initial deflection of spring s (f=0.5)

to maximize the energy dissipation rate exists around s=0.3 at which the reflection coefficient shows the minimum. As seen in the figure, the increase in the friction coefficient somewhat improve the agreement with the experimental results, which is also seen in Fig. 14.

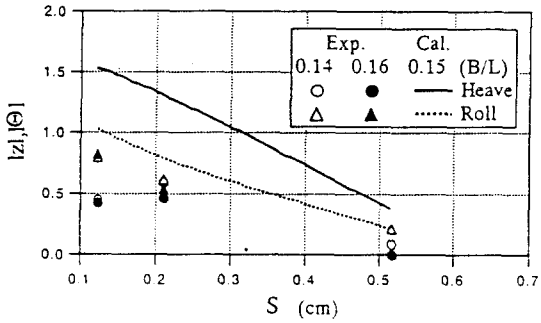

Fig. 14 Heave and roll amplitudes as functions of initial deflection of spring s (f=0.5)

4. CONCLUDING REMARKS

In this paper, the nonlinear and linear models are proposed for the calculation of wave transformation and the motions of a pile-supported floating body. The friction forces occurring between the rollers and the piles are idealized as the Coulomb friction and linearized by using the equivalent damping coefficient. Although the models must be further modified by examining the characteristics of the friction forces in detail, it is at least confirmed that the significant energy dissipation can be expected for such pile-supported floating structures as treated in this study.

ACKNOWLEDGEMENTS

This work was supported in part by the Korea Science and Engineering Foundation (KOSEF) through the Research Center for Ocean

Industrial Development at Pukyong National University.

5. REFERENCES

1) Kim, H.T., Sawaragi, T., and Aoki, S., "Wave control by pile-supported floating breakwaters", Proc. of the fourth International Offshore and Polar Engineering Conference, Osaka, vol. III, pp.545-549, 1994

2) Yoshida, A., Kojima, H., Tsurumoto, Y., "A collocation method of matched eigenfunction expansions on the boundary-value problem of wave-structure interactions", Proc. of JSCE, No.417/II-13, pp.265-274 (in Japanese), 1990